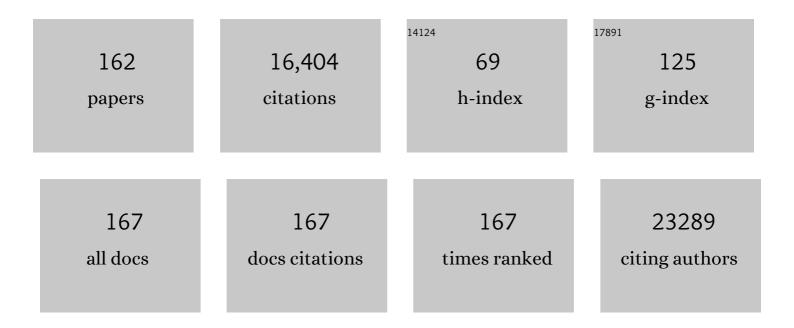
Liang Zhou

List of Publications by Year in descending order

Source: https://exaly.com/author-pdf/466039/publications.pdf Version: 2024-02-01



#	Article	IF	CITATIONS
1	Aberrant expression profiles and bioinformatic analysis of CAFâ€derived exosomal miRNAs from three moderately differentiated supraglottic LSCC patients. Journal of Clinical Laboratory Analysis, 2022, 36, e24108.	0.9	8
2	<i>PURPL</i> directly modulates ULK1 phosphorylation to inhibit autophagic cell death. , 2022, 1, 17-20.		0
3	Dabigatran versus aspirin for stroke prevention after cryptogenic stroke with patent foramen ovale: A prospective study. Clinical Neurology and Neurosurgery, 2022, 215, 107189.	0.6	3
4	Fine-Needle Pricking Test of the Parathyroid Gland during Thyroid Surgery in Predicting Parathyroid Function. International Journal of Endocrinology, 2022, 2022, 1-9.	0.6	2
5	Frameshift mutation of <i>Timm8a1</i> gene in mouse leads to an abnormal mitochondrial structure in the brain, correlating with hearing and memory impairment. Journal of Medical Genetics, 2021, 58, 619-627.	1.5	12
6	A nomogram for predicting occult lymph node metastasis in early hypopharyngeal cancer with cN0. European Archives of Oto-Rhino-Laryngology, 2021, 278, 3515-3522.	0.8	10
7	Upregulating hsa-miR-128a Increased the Effects of Pembrolizumab on Laryngeal Cancer Cells via the p53 Pathway. BioMed Research International, 2021, 2021, 1-6.	0.9	4
8	Preoperative tracheotomy as reflection of tumor size impacting oncologic outcomes of patients with advanced stage glottic carcinoma. European Archives of Oto-Rhino-Laryngology, 2021, 278, 4943-4950.	0.8	1
9	Author's reply regarding the letter to the editor about our article: A nomogram for predicting occult lymph node metastasis in early hypopharyngeal cancer with cN0. European Archives of Oto-Rhino-Laryngology, 2021, 278, 3603-3603.	0.8	0
10	Carbon nitride nanotubes with in situ grafted hydroxyl groups for highly efficient spontaneous H2O2 production. Applied Catalysis B: Environmental, 2021, 288, 119993.	10.8	102
11	Charcot–Marie–Tooth Disease With Episodic Rhabdomyolysis Due to Two Novel Mutations in the β Subunit of Mitochondrial Trifunctional Protein and Effective Response to Modified Diet Therapy. Frontiers in Neurology, 2021, 12, 694966.	1.1	1
12	PURPL represses autophagic cell death to promote cutaneous melanoma by modulating ULK1 phosphorylation. Cell Death and Disease, 2021, 12, 1070.	2.7	23
13	Prognostic values of preoperative plateletâ€to″ymphocyte ratio and plateletâ€related indices in advanced hypopharyngeal squamous cell carcinoma. Clinical Otolaryngology, 2020, 45, 221-230.	0.6	4
14	Early and long-term outcomes of argatroban use in patients with acute noncardioembolic stroke. Clinical Neurology and Neurosurgery, 2020, 198, 106233.	0.6	7
15	Radiosensitivity-Related Genes and Clinical Characteristics of Nasopharyngeal Carcinoma. BioMed Research International, 2020, 2020, 1-13.	0.9	4
16	Long noncoding RNA SAM promotes myoblast proliferation through stabilizing Sugt1 and facilitating kinetochore assembly. Nature Communications, 2020, 11, 2725.	5.8	23
17	Exosomal Small RNA Sequencing Uncovers Dose-Specific MiRNA Markers for Ionizing Radiation Exposure. Dose-Response, 2020, 18, 155932582092673.	0.7	6
18	Recurrent panic attack and bilateral hippocampus lesions as main manifestation in an autoimmune encephalitis associated with primary biliary cirrhosis. Chinese Medical Journal, 2020, 133, 369-371.	0.9	1

#	Article	IF	CITATIONS
19	lschemiaâ€reperfusion injury of brain induces endothelialâ€mesenchymal transition and vascular fibrosis via activating letâ€7i/TGFâ€Î²R1 doubleâ€negative feedback loop. FASEB Journal, 2020, 34, 7178-7191.	0.2	24
20	HOXA9 Transcriptionally Promotes Apoptosis and Represses Autophagy by Targeting NF-κB in Cutaneous Squamous Cell Carcinoma. Cells, 2019, 8, 1360.	1.8	24
21	Assessment of the therapeutic accuracy of cone beam computed tomography‑guided nasopharyngeal carcinoma radiotherapy. Oncology Letters, 2019, 18, 1071-1080.	0.8	3
22	MALAT1-KTN1-EGFR regulatory axis promotes the development of cutaneous squamous cell carcinoma. Cell Death and Differentiation, 2019, 26, 2061-2073.	5.0	44
23	Silicon oxides: a promising family of anode materials for lithium-ion batteries. Chemical Society Reviews, 2019, 48, 285-309.	18.7	685
24	Gefitinib‑mediated apoptosis is enhanced via inhibition of autophagy by chloroquine diphosphate in cutaneous squamous cell carcinoma cells. Oncology Letters, 2019, 18, 368-374.	0.8	7
25	Pretreatment Serum Uric Acid as an Efficient Predictor of Prognosis in Men with Laryngeal Squamous Cell Cancer: A Retrospective Cohort Study. Oxidative Medicine and Cellular Longevity, 2019, 2019, 1-12.	1.9	7
26	DIAPH1 Is Upregulated and Inhibits Cell Apoptosis through ATR/p53/Caspase-3 Signaling Pathway in Laryngeal Squamous Cell Carcinoma. Disease Markers, 2019, 2019, 1-10.	0.6	25
27	Clinical behaviours and prognoses of high- and low-risk parotid malignancies based on histology. European Archives of Oto-Rhino-Laryngology, 2019, 276, 497-503.	0.8	9
28	Chloroquine promotes gefitinib‑induced apoptosis by inhibiting protective autophagy in cutaneous squamous cell carcinoma. Molecular Medicine Reports, 2019, 20, 4855-4866.	1.1	9
29	HOXA9 inhibits HIF-1α-mediated glycolysis through interacting with CRIP2 to repress cutaneous squamous cell carcinoma development. Nature Communications, 2018, 9, 1480.	5.8	90
30	Anions induced evolution of Co3X4 (X = O, S, Se) as sodium-ion anodes: The influences of electronic structure, morphology, electrochemical property. Nano Energy, 2018, 48, 617-629.	8.2	227
31	Highly Durable Na ₂ V ₆ O ₁₆ ·1.63H ₂ O Nanowire Cathode for Aqueous Zinc-Ion Battery. Nano Letters, 2018, 18, 1758-1763.	4.5	568
32	Heterostructured Bi ₂ S ₃ –Bi ₂ O ₃ Nanosheets with a Built-In Electric Field for Improved Sodium Storage. ACS Applied Materials & Interfaces, 2018, 10, 7201-7207.	4.0	153
33	Exosomal small RNA sequencing uncovers the microRNA dose markers for power frequency electromagnetic field exposure. Biomarkers, 2018, 23, 315-327.	0.9	6
34	Bottomâ€Up Confined Synthesis of Nanorodâ€inâ€Nanotube Structured Sb@N for Durable Lithium and Sodium Storage. Advanced Energy Materials, 2018, 8, 1703237.	10.2	192
35	Graphene oxide-decorated Fe2(MoO4)3 microflowers as a promising anode for lithium and sodium storage. Nano Research, 2018, 11, 1285-1293.	5.8	25
36	Ultrafine Nickelâ€Nanoparticleâ€Enabled SiO ₂ Hierarchical Hollow Spheres for Highâ€Performance Lithium Storage. Advanced Functional Materials, 2018, 28, 1704561.	7.8	193

#	Article	IF	CITATIONS
37	MoB/g ₃ N ₄ Interface Materials as a Schottky Catalyst to Boost Hydrogen Evolution. Angewandte Chemie - International Edition, 2018, 57, 496-500.	7.2	308
38	Tailoring porous carbon spheres for supercapacitors. Nanoscale, 2018, 10, 21604-21616.	2.8	101
39	TLR4 signaling pathway mediates the LPS/ischemia-induced expression of monocytechemotactic protein-induced protein 1 in microglia. Neuroscience Letters, 2018, 686, 33-40.	1.0	17
40	Ni foam supported NiO nanosheets as high-performance free-standing electrodes for hybrid supercapacitors and Ni–Zn batteries. Journal of Materials Chemistry A, 2018, 6, 19488-19494.	5.2	73
41	The Marriage of the FeN ₄ Moiety and MXene Boosts Oxygen Reduction Catalysis: Fe 3d Electron Delocalization Matters. Advanced Materials, 2018, 30, e1803220.	11.1	289
42	Boosting the Deep Discharging/Charging Lithium Storage Performances of Li ₃ VO ₄ through Double-Carbon Decoration. ACS Applied Materials & Interfaces, 2018, 10, 23938-23944.	4.0	45
43	Ultrafine SiO _x /C nanospheres and their pomegranate-like assemblies for high-performance lithium storage. Journal of Materials Chemistry A, 2018, 6, 14903-14909.	5.2	115
44	Cell permeable HMGB1-binding heptamer peptide ameliorates neurovascular complications associated with thrombolytic therapy in rats with transient ischemic stroke. Journal of Neuroinflammation, 2018, 15, 237.	3.1	31
45	Nickel Chelate Derived NiS ₂ Decorated with Bifunctional Carbon: An Efficient Strategy to Promote Sodium Storage Performance. Advanced Functional Materials, 2018, 28, 1803690.	7.8	104
46	Eotaxin‑1 and MCP‑1 serve as circulating indicators in response to power frequency electromagnetic field exposure in mice. Molecular Medicine Reports, 2018, 18, 2832-2840.	1.1	0
47	Association of lower leukocyte count before thrombolysis with early neurological improvement in acute ischemic stroke patients. Journal of Clinical Neuroscience, 2018, 56, 44-49.	0.8	15
48	Tailored Yolk–Shell Sn@C Nanoboxes for Highâ€Performance Lithium Storage. Advanced Functional Materials, 2017, 27, 1606023.	7.8	173
49	Copper silicate nanotubes anchored on reduced graphene oxide for long-life lithium-ion battery. Energy Storage Materials, 2017, 7, 152-156.	9.5	67
50	Intricate Hollow Structures: Controlled Synthesis and Applications in Energy Storage and Conversion. Advanced Materials, 2017, 29, 1602914.	11.1	523
51	Low-crystalline iron oxide hydroxide nanoparticle anode for high-performance supercapacitors. Nature Communications, 2017, 8, 14264.	5.8	588
52	Methyl-functionalized MoS ₂ nanosheets with reduced lattice breathing for enhanced pseudocapacitive sodium storage. Physical Chemistry Chemical Physics, 2017, 19, 13696-13702.	1.3	62
53	Thermal Induced Strain Relaxation of 1D Iron Oxide for Solid Electrolyte Interphase Control and Lithium Storage Improvement. Advanced Energy Materials, 2017, 7, 1601582.	10.2	73
54	A Molecular Switch Regulating Cell Fate Choice between Muscle Progenitor Cells and Brown Adipocytes. Developmental Cell, 2017, 41, 382-391.e5.	3.1	48

#	Article	IF	CITATIONS
55	Mass Production of Monodisperse Carbon Microspheres with Sizeâ€Dependent Supercapacitor Performance via Aqueous Selfâ€Catalyzed Polymerization. ChemPlusChem, 2017, 82, 872-878.	1.3	46
56	Facile synthesis of MoO 2 @C nanoflowers as anode materials for sodium-ion batteries. Materials Research Bulletin, 2017, 94, 122-126.	2.7	19
57	New-type K0.7Fe0.5Mn0.5O2 cathode with an expanded and stabilized interlayer structure for high-capacity sodium-ion batteries. Nano Energy, 2017, 35, 71-78.	8.2	60
58	Malat1 regulates myogenic differentiation and muscle regeneration through modulating MyoD transcriptional activity. Cell Discovery, 2017, 3, 17002.	3.1	86
59	Interconnected LiCuVO ₄ networks with in situ Cu generation as high-performance lithium-ion battery anode. Physical Chemistry Chemical Physics, 2017, 19, 13341-13347.	1.3	15
60	Facet-Selective Deposition of FeO _{<i>x</i>} on α-MoO ₃ Nanobelts for Lithium Storage. ACS Applied Materials & Interfaces, 2017, 9, 39425-39431.	4.0	36
61	Let-7i attenuates human brain microvascular endothelial cell damage in oxygen glucose deprivation model by decreasing toll-like receptor 4 expression. Biochemical and Biophysical Research Communications, 2017, 493, 788-793.	1.0	28
62	Plasma let-7i and miR-15a expression are associated with the effect of recombinant tissue plasminogen activator treatment in acute ischemic stroke patients. Thrombosis Research, 2017, 158, 121-125.	0.8	16
63	Aerosol synthesis of trivalent titanium doped titania/carbon composite microspheres with superior sodium storage performance. Nano Research, 2017, 10, 4351-4359.	5.8	47
64	Zn/V ₂ O ₅ Aqueous Hybrid-Ion Battery with High Voltage Platform and Long Cycle Life. ACS Applied Materials & Interfaces, 2017, 9, 42717-42722.	4.0	401
65	Metal–organic framework derived carbon-confined Ni ₂ P nanocrystals supported on graphene for an efficient oxygen evolution reaction. Chemical Communications, 2017, 53, 8372-8375.	2.2	184
66	Porous and Low-Crystalline Manganese Silicate Hollow Spheres Wired by Graphene Oxide for High-Performance Lithium and Sodium Storage. ACS Applied Materials & Interfaces, 2017, 9, 24584-24590.	4.0	79
67	Facile Synthesis of Bi ₂ S ₃ @SiO ₂ Core-Shell Microwires as High-Performance Anode Materials for Lithium-Ion Batteries. Journal of the Electrochemical Society, 2017, 164, A6110-A6115.	1.3	26
68	Loss of BAX by miR-365 Promotes Cutaneous Squamous Cell Carcinoma Progression by Suppressing Apoptosis. International Journal of Molecular Sciences, 2017, 18, 1157.	1.8	30
69	Down-regulation of ABCG2 and ABCB4 transporters in the placenta of rats exposed to cadmium. Oncotarget, 2016, 7, 38154-38163.	0.8	15
70	Engineering Iron Oxide Hollow Nanospheres to Enhance Antimicrobial Property: Understanding the Cytotoxic Origin in Organic Rich Environment. Advanced Functional Materials, 2016, 26, 5408-5418.	7.8	46
71	Layerâ€byâ€Layer Na ₃ V ₂ (PO ₄) ₃ Embedded in Reduced Graphene Oxide as Superior Rate and Ultralongâ€Life Sodiumâ€Ion Battery Cathode. Advanced Energy Materials, 2016, 6, 1600389.	10.2	282
72	A High-Rate V ₂ O ₅ Hollow Microclew Cathode for an All-Vanadium-Based Lithium-Ion Full Cell. Small, 2016, 12, 1082-1090.	5.2	55

#	Article	IF	CITATIONS
73	Polypyrroleâ€Coated Zinc Ferrite Hollow Spheres with Improved Cycling Stability for Lithiumâ€Ion Batteries. Small, 2016, 12, 3732-3737.	5.2	102
74	Binder-Free TiO2 Monolith-Packed Pipette Tips for the Enrichment of Phosphorylated Peptides. Australian Journal of Chemistry, 2016, 69, 1396.	0.5	5
75	Ultralong Sb ₂ Se ₃ Nanowire-Based Free-Standing Membrane Anode for Lithium/Sodium Ion Batteries. ACS Applied Materials & Interfaces, 2016, 8, 35219-35226.	4.0	139
76	In operando observation of temperature-dependent phase evolution in lithium-incorporation olivine cathode. Nano Energy, 2016, 22, 406-413.	8.2	31
77	Surfactant-Free Assembly of Mesoporous Carbon Hollow Spheres with Large Tunable Pore Sizes. ACS Nano, 2016, 10, 4579-4586.	7.3	374
78	Kinetically Controlled Assembly of Nitrogenâ€Doped Invaginated Carbon Nanospheres with Tunable Mesopores. Chemistry - A European Journal, 2016, 22, 14962-14967.	1.7	21
79	Encapsulation of selenium sulfide in double-layered hollow carbon spheres as advanced electrode material for lithium storage. Nano Research, 2016, 9, 3725-3734.	5.8	45
80	Carbon-coated hierarchical NaTi2(PO4)3 mesoporous microflowers with superior sodium storage performance. Nano Energy, 2016, 28, 224-231.	8.2	139
81	Prodigiosin inhibits Wnt/β-catenin signaling and exerts anticancer activity in breast cancer cells. Proceedings of the National Academy of Sciences of the United States of America, 2016, 113, 13150-13155.	3.3	151
82	Graphene Oxide Templated Growth and Superior Lithium Storage Performance of Novel Hierarchical Co ₂ V ₂ O ₇ Nanosheets. ACS Applied Materials & Interfaces, 2016, 8, 2812-2818.	4.0	74
83	Genome-wide RNA-seq and ChIP-seq reveal Linc-YY1 function in regulating YY1/PRC2 activity during skeletal myogenesis. Genomics Data, 2016, 7, 247-249.	1.3	8
84	Acetylene Black Induced Heterogeneous Growth of Macroporous CoV ₂ O ₆ Nanosheet for High-Rate Pseudocapacitive Lithium-Ion Battery Anode. ACS Applied Materials & Interfaces, 2016, 8, 7139-7146.	4.0	81
85	Antimony nanoparticles anchored in three-dimensional carbon network as promising sodium-ion battery anode. Journal of Power Sources, 2016, 304, 340-345.	4.0	109
86	Novel K ₃ V ₂ (PO ₄) ₃ /C Bundled Nanowires as Superior Sodiumâ€Ion Battery Electrode with Ultrahigh Cycling Stability. Advanced Energy Materials, 2015, 5, 1500716.	10.2	150
87	Linc-YY1 promotes myogenic differentiation and muscle regeneration through an interaction with the transcription factor YY1. Nature Communications, 2015, 6, 10026.	5.8	168
88	Unilateral Symptomatic Intracranial Arterial Stenosis and Myopathy in an Adolescent with Graves Disease: A Case Report of an High-resolution Magnetic Resonance Imaging Study. Journal of Stroke and Cerebrovascular Diseases, 2015, 24, e49-e52.	0.7	2
89	Encapsulation of α-Fe ₂ O ₃ nanoparticles in graphitic carbon microspheres as high-performance anode materials for lithium-ion batteries. Nanoscale, 2015, 7, 3270-3275.	2.8	82

6

#	Article	IF	CITATIONS
91	Self-Organized Mesostructured Hollow Carbon Nanoparticles via a Surfactant-Free Sequential Heterogeneous Nucleation Pathway. Chemistry of Materials, 2015, 27, 6297-6304.	3.2	99
92	microRNA-365-targeted nuclear factor I/B transcriptionally represses cyclin-dependent kinase 6 and 4 to inhibit the progression of cutaneous squamous cell carcinoma. International Journal of Biochemistry and Cell Biology, 2015, 65, 182-191.	1.2	30
93	Mesoporous Li ₃ VO ₄ /C Submicronâ€Ellipsoids Supported on Reduced Graphene Oxide as Practical Anode for Highâ€Power Lithiumâ€lon Batteries. Advanced Science, 2015, 2, 1500284.	5.6	99
94	Nitrogen-doped ordered mesoporous carbon single crystals: aqueous organic–organic self-assembly and superior supercapacitor performance. Journal of Materials Chemistry A, 2015, 3, 24041-24048.	5.2	96
95	Facile synthesis of reduced graphene oxide wrapped nickel silicate hierarchical hollow spheres for long-life lithium-ion batteries. Journal of Materials Chemistry A, 2015, 3, 19427-19432.	5.2	72
96	Lattice Breathing Inhibited Layered Vanadium Oxide Ultrathin Nanobelts for Enhanced Sodium Storage. ACS Applied Materials & Interfaces, 2015, 7, 18211-18217.	4.0	94
97	Shaping Nanoparticles with Hydrophilic Compositions and Hydrophobic Properties as Nanocarriers for Antibiotic Delivery. ACS Central Science, 2015, 1, 328-334.	5.3	65
98	Synthesis of Magnesium Oxide Hierarchical Microspheres: A Dual-Functional Material for Water Remediation. ACS Applied Materials & Interfaces, 2015, 7, 21278-21286.	4.0	124
99	Dysbiosis of Gut Microbiota With Reduced Trimethylamineâ€Nâ€Oxide Level in Patients With Largeâ€Artery Atherosclerotic Stroke or Transient Ischemic Attack. Journal of the American Heart Association, 2015, 4, .	1.6	486
100	Copper Silicate Hydrate Hollow Spheres Constructed by Nanotubes Encapsulated in Reduced Graphene Oxide as Long-Life Lithium-Ion Battery Anode. ACS Applied Materials & Interfaces, 2015, 7, 26572-26578.	4.0	82
101	The p53-induced lincRNA-p21 derails somatic cell reprogramming by sustaining H3K9me3 and CpG methylation at pluripotency gene promoters. Cell Research, 2015, 25, 80-92.	5.7	160
102	Platinum Nanoparticles Encapsulated in Carbon Microspheres: Toward Electro-Catalyzing Glucose with High Activity and Stability. Electrochimica Acta, 2015, 151, 326-331.	2.6	16
103	Paraformaldehyde Fixation May Lead to Misinterpretation of the Subcellular Localization of Plant High Mobility Group Box Proteins. PLoS ONE, 2015, 10, e0135033.	1.1	8
104	miR-365 Promotes Cutaneous Squamous Cell Carcinoma (CSCC) through Targeting Nuclear Factor I/B (NFIB). PLoS ONE, 2014, 9, e100620.	1.1	65
105	Comparison of percutaneous cryoablation with microwave ablation in a porcine liver model. Cryobiology, 2014, 68, 194-199.	0.3	8
106	Fabrication of ordered mesoporous carbon hollow fiber membranes via a confined soft templating approach. Journal of Materials Chemistry A, 2014, 2, 4144-4149.	5.2	22
107	Tailoring the Void Size of Iron Oxide@Carbon Yolk–Shell Structure for Optimized Lithium Storage. Advanced Functional Materials, 2014, 24, 4337-4342.	7.8	212
108	A combo-pore approach for the programmable extraction of peptides/proteins. Nanoscale, 2014, 6, 5121-5125.	2.8	31

#	Article	IF	CITATIONS
109	Highly crystallized Fe2O3nanocrystals on graphene: a lithium ion battery anode material with enhanced cycling. RSC Advances, 2014, 4, 495-499.	1.7	37
110	A Novel Wnt Regulatory Axis in Endometrioid Endometrial Cancer. Cancer Research, 2014, 74, 5103-5117.	0.4	114
111	Cheap and scalable synthesis of α-Fe2O3 multi-shelled hollow spheres as high-performance anode materials for lithium ion batteries. Chemical Communications, 2013, 49, 8695.	2.2	192
112	Confinement of Chemisorbed Phosphates in a Controlled Nanospace with Threeâ€Dimensional Mesostructures. Chemistry - A European Journal, 2013, 19, 5578-5585.	1.7	16
113	Genome-wide survey by ChIP-seq reveals YY1 regulation of lincRNAs in skeletal myogenesis. EMBO Journal, 2013, 32, 2575-2588.	3.5	138
114	c-Jun NH2-terminal Kinase (JNK)-interacting Protein-3 (JIP3) Regulates Neuronal Axon Elongation in a Kinesin- and JNK-dependent Manner. Journal of Biological Chemistry, 2013, 288, 14531-14543.	1.6	53
115	A novel miR-193a-5p-YY1-APC regulatory axis in human endometrioid endometrial adenocarcinoma. Oncogene, 2013, 32, 3432-3442.	2.6	71
116	Designed synthesis of LiMn ₂ O ₄ microspheres with adjustable hollow structures for lithium-ion battery applications. Journal of Materials Chemistry A, 2013, 1, 837-842.	5.2	56
117	Low-cost and large-scale synthesis of functional porous materials for phosphate removal with high performance. Nanoscale, 2013, 5, 6173.	2.8	60
118	Laser Engineered Graphene Paper for Mass Spectrometry Imaging. Scientific Reports, 2013, 3, 1415.	1.6	44
119	Loss of miR-29 in Myoblasts Contributes to Dystrophic Muscle Pathogenesis. Molecular Therapy, 2012, 20, 1222-1233.	3.7	111
120	A Novel Target of MicroRNA-29, Ring1 and YY1-binding Protein (Rybp), Negatively Regulates Skeletal Myogenesis. Journal of Biological Chemistry, 2012, 287, 25255-25265.	1.6	92
121	Self-assembly of monodispersed silica nano-spheres with a closed-pore mesostructure. Journal of Materials Chemistry, 2012, 22, 11523.	6.7	18
122	Facile preparation of ZnMn ₂ O ₄ hollow microspheres as high-capacity anodes for lithium-ion batteries. Journal of Materials Chemistry, 2012, 22, 827-829.	6.7	236
123	A Novel YY1-miR-1 Regulatory Circuit in Skeletal Myogenesis Revealed by Genome-Wide Prediction of YY1-miRNA Network. PLoS ONE, 2012, 7, e27596.	1.1	88
124	Inhibition of miR-29 by TGF-beta-Smad3 Signaling through Dual Mechanisms Promotes Transdifferentiation of Mouse Myoblasts into Myofibroblasts. PLoS ONE, 2012, 7, e33766.	1.1	120
125	Unusual Formation of Singleâ€Crystal Manganese Sulfide Microboxes Coâ€mediated by the Cubic Crystal Structure and Shape. Angewandte Chemie - International Edition, 2012, 51, 7267-7270.	7.2	103
126	Arrays of ultrafine CuS nanoneedles supported on a CNT backbone for application in supercapacitors. Journal of Materials Chemistry, 2012, 22, 7851.	6.7	253

#	Article	IF	CITATIONS
127	A simple approach to prepare monodisperse mesoporous silica nanospheres with adjustable sizes. Journal of Colloid and Interface Science, 2012, 376, 67-75.	5.0	71
128	Change in hepatocyte growth factor concentration promote mesenchymal stem cellâ€mediated osteogenic regeneration. Journal of Cellular and Molecular Medicine, 2012, 16, 1260-1273.	1.6	41
129	Expression of an apoplastâ€localized BURPâ€domain protein from soybean (GmRD22) enhances tolerance towards abiotic stress. Plant, Cell and Environment, 2012, 35, 1932-1947.	2.8	86
130	Double‧helled CoMn ₂ O ₄ Hollow Microcubes as High apacity Anodes for Lithiumâ€lon Batteries. Advanced Materials, 2012, 24, 745-748.	11.1	665
131	Metal Oxide Hollow Nanostructures for Lithiumâ€ion Batteries. Advanced Materials, 2012, 24, 1903-1911.	11.1	1,414
132	LiNi _{0.5} Mn _{1.5} O ₄ Hollow Structures as Highâ€Performance Cathodes for Lithiumâ€Ion Batteries. Angewandte Chemie - International Edition, 2012, 51, 239-241.	7.2	340
133	Hierarchical Cu ₄ V _{2.15} O _{9.38} micro-/nanostructures: a lithium intercalating electrode material. Nanoscale, 2011, 3, 999-1003.	2.8	24
134	A systematic study of long-range ordered 3D-SBA-15 materials by electron tomography. New Journal of Chemistry, 2011, 35, 2456.	1.4	24
135	Interconnected MoO ₂ Nanocrystals with Carbon Nanocoating as High-Capacity Anode Materials for Lithium-ion Batteries. ACS Applied Materials & Interfaces, 2011, 3, 4853-4857.	4.0	167
136	Extensive Inspection of an Unconventional Mesoporous Silica Material at All Length-Scales. Chemistry of Materials, 2011, 23, 229-238.	3.2	14
137	A designed nanoporous material for phosphate removal with high efficiency. Journal of Materials Chemistry, 2011, 21, 2489.	6.7	127
138	Magnetic-field induced formation of 1D Fe3O4/C/CdS coaxial nanochains as highly efficient and reusable photocatalysts for water treatment. Journal of Materials Chemistry, 2011, 21, 18359.	6.7	145
139	Small Mesoporous Silica Nanoparticles as Carriers for Enhanced Photodynamic Therapy. Chemistry - an Asian Journal, 2011, 6, 2332-2338.	1.7	23
140	Synthesis and in-vitro bioactivity of mesoporous bioactive glasses with tunable macropores. Microporous and Mesoporous Materials, 2011, 143, 157-165.	2.2	23
141	A Facile One‣tep Solvothermal Synthesis of SnO ₂ /Graphene Nanocomposite and Its Application as an Anode Material for Lithiumâ€ion Batteries. ChemPhysChem, 2011, 12, 278-281.	1.0	111
142	A silanol protection mechanism: Understanding the decomposition behavior of surfactants in mesostructured solids. Journal of Materials Research, 2011, 26, 804-814.	1.2	11
143	Synthesis of highly ordered and hydrothermally stable mesoporous materials using sodium silicate as a precursor. Materials Letters, 2010, 64, 1543-1545.	1.3	12
144	Rice Hypersensitive Induced Reaction Protein 1 (OsHIR1) associates with plasma membrane and triggers hypersensitive cell death. BMC Plant Biology, 2010, 10, 290.	1.6	70

#	Article	IF	CITATIONS
145	An Ancient P-Loop GTPase in Rice Is Regulated by a Higher Plant-specific Regulatory Protein. Journal of Biological Chemistry, 2010, 285, 37359-37369.	1.6	41
146	α-MoO ₃ Nanobelts: A High Performance Cathode Material for Lithium Ion Batteries. Journal of Physical Chemistry C, 2010, 114, 21868-21872.	1.5	248
147	Mo _{<i>x</i>} W _{1â^<i>x</i>} O ₃ ·0.33H ₂ O Solid Solutions with Tunable Band Gaps. Journal of Physical Chemistry C, 2010, 114, 20947-20954.	1.5	64
148	Nanosheet-Based Bi ₂ Mo _{<i>x</i>} W _{1â^'<i>x</i>} O ₆ Solid Solutions with Adjustable Band Gaps and Enhanced Visible-Light-Driven Photocatalytic Activities. Journal of Physical Chemistry C, 2010, 114, 18812-18818.	1.5	83
149	Synthesis of urchin-like CdWO4 microspheres via a facile template free hydrothermal method. CrystEngComm, 2010, 12, 3019.	1.3	26
150	Electrochemical Properties of Ordered Mesoporous Carbon Film Adsorbed onto a Selfâ€Assembled Alkanethiol Monolayer on Gold Electrode. Electroanalysis, 2009, 21, 184-189.	1.5	24
151	A novel simple extracellular leucineâ€rich repeat (eLRR) domain protein from rice (OsLRR1) enters the endosomal pathway and interacts with the hypersensitiveâ€induced reaction protein 1 (OsHIR1). Plant, Cell and Environment, 2009, 32, 1804-1820.	2.8	44
152	Simultaneous determination of dopamine, ascorbic acid and uric acid on ordered mesoporous carbon/Nafion composite film. Journal of Electroanalytical Chemistry, 2009, 625, 82-87.	1.9	151
153	On the Equilibrium of Helical Nanostructures with Ordered Mesopores. Journal of Physical Chemistry B, 2009, 113, 16178-16183.	1.2	7
154	New Understanding and Simple Approach to Synthesize Highly Hydrothermally Stable and Ordered Mesoporous Materials. Chemistry of Materials, 2009, 21, 5413-5425.	3.2	69
155	Nanosheets-Based Rhombohedral In ₂ O ₃ 3D Hierarchical Microspheres: Synthesis, Growth Mechanism, and Optical Properties. Journal of Physical Chemistry C, 2009, 113, 10511-10516.	1.5	49
156	Solving Complex Concentric Circular Mesostructures by Using Electron Tomography. Angewandte Chemie - International Edition, 2008, 47, 6670-6673.	7.2	24
157	Mesoporous bioactive glasses for controlled drug release. Microporous and Mesoporous Materials, 2008, 109, 210-215.	2.2	113
158	Comprehensive understanding on the formation of highly ordered mesoporous tungsten oxides by X-ray diffraction and Raman spectroscopy. Microporous and Mesoporous Materials, 2008, 109, 248-257.	2.2	48
159	Green Synthesis of Hexagonal-Shaped WO ₃ ·0.33H ₂ O Nanodiscs Composed of Nanosheets. Crystal Growth and Design, 2008, 8, 3993-3998.	1.4	94
160	Organosilica Multilamellar Vesicles with Tunable Number of Layers and Sponge-Like Walls via One Surfactant Templating. Chemistry of Materials, 2008, 20, 6238-6243.	3.2	48
161	Synthesis of Enantiomorphic Excessive Helical Mesoporous Silicas Using Chiral Molecular Dopants. Chemistry Letters, 2008, 37, 1160-1161.	0.7	8
162	Easy synthesis and supercapacities of highly ordered mesoporous polyacenes/carbons. Carbon, 2006, 44, 1601-1604.	5.4	29